Materials Physics and Mechanics. 2023;51(7): 42-62
Research article
http://dx.doi.org/10.18149/MPM.5172023_6

Submitted: September 4, 2023
Approved: September 25, 2023
Accepted: November 3, 2023

Elastic properties of additively produced metamaterials based on lattice structures

A.I. Borovkov [1], L.B. Maslov [1,2], M.A. Zhmaylo [1]✉, F.D. Tarasenko [1], L.S. Nezhinskaya [1]

[1] Peter the Great St. Petersburg Polytechnic University, St. Petersburg, Russia

[2] Ivanovo State Power Engineering University, Ivanovo, Russia

✉ zhmaylo@compmechlab.com

Abstract. The paper considers seven types of lattice structures of different topologies, which are periodic unit cells of metamaterials to be manufactured by additive technologies. We carried out finite-element analysis of lattice structures with varying thicknesses of elementary beams comprising the cells and varying initial symmetric shapes. The effective elastic properties of metamaterials as continuous media were calculated by the method of direct numerical homogenization with periodic boundary conditions. The dependences between elastic properties and characteristic parameters determining the topology of cells were established. Some types of lattices were found to exhibit auxetic properties in a certain range of topological parameters.

Keywords: metamaterials; lattice structures; elastic moduli; finite element analysis; homogenization

Acknowledgements. *This work has been supported by the Russian Science Foundation grant No. 23-19-00882, https://rscf.ru/project/23-19-00882/.*

Citation: Borovkov AI, Maslov LB, Zhmaylo MA, Tarasenko FD, Nezhinskaya LS. Elastic properties of additively produced metamaterials based on lattice structures. *Materials Physics and Mechanics*. 2023;51(7): 42-62. DOI: 10.18149/MPM.5172023_6.

Introduction

Over the last decade, additive technologies, as a group of manufacturing technologies with a wide range of capabilities and few limitations, have made it possible to produce complex metal and polymer parts and components that could not previously be produced by conventional material processing technologies [1]. Metamaterials, whose physical and mechanical properties can be controlled by changing the shape and parameters of a unit cell, are an example of such structures.

Metamaterials are understood as artificially designed multiscale structures formed by periodically repeating basic cells of relatively small size, fine-tuned to ensure that the physical and mechanical behaviour of the structure at the macro-level is that of a continuous material. A characteristic example of a metamaterial is a periodic lattice structure, which is formed by duplicating a unit cell in the directions of three non-coplanar vectors on which a parallelepiped describing the boundary of the unit cell is built [2]. Such a structure has a three-dimensional periodic topology, whose step of repetition depends on the geometric dimensions of the unit cell. The metamaterials can also include porous media with a complicated multiscale system of pore channels [3].

Since typical unit cells have complex topology, the parts integrating metamaterials can only be manufactured by additive technologies, primarily powder-based laser 3D printing. It is the specific topology and variable shape of the elementary structural cell that gives the metamaterial unique physical and mechanical properties at the macro-level, unattainable for conventional homogeneous materials. In this case, the elastic properties of the metamaterial at the macro-level are assumed to be the effective properties of the structural cell as a part of a periodic array along three axes of the global coordinate system. Thus, a metamaterial can be characterized as an additively produced material consisting of a large number of unit cells whose size is much smaller than the size of a part made of the metamaterial.

The effective physical and mechanical properties of the metamaterial, which are considerably different from the properties of the solid material from which the periodic structure is fabricated, can be determined using the homogenization procedure performed for the representative volume element (RVE) of the metamaterial [4]. In the case of a metamaterial formed by arrays of unit cells along three Cartesian axes, the RVE is a structure of minimal volume, containing the characteristic geometry of the material repeating with a certain step, so it can be regarded as a periodicity cell from the standpoint of theory of heterogeneous and composite materials.

The dependences of effective elastic properties of metamaterials on the topological features of the structure at the meso-level are a popular subject for research in mechanics of heterogeneous continuous media [5]. The main objective of this research is to establish the approaches to designing the mechanical properties of the structure by varying the topology of the unit cell by new unconventional techniques [6]. In particular, the numerical analysis of the mechanical properties of the unit cell was carried out in [7] by the homogenization method with varying topological parameters of the unit cell.

Recent developments in the field of metamaterials for special applications are outlined in [8], covering ultra-lightweight, ultra-stiff and ultra-strong materials, with emphasis placed on metamaterials with negative compressibility and negative stiffness. The current understanding of the structure and mechanical behaviour of cellular materials with low effective density, and how they can be used in the design of engineering structures, is discussed in [9].

Numerous studies deal with the influence of topological properties of metamaterials on their mechanical performance, considering different types of unit cells with varied effective porosity [10]. Some papers introduce hypotheses about the analytical dependences between the mechanical constants and the effective porosity obeying a power law [11]. However, such dependencies do not take into account a wide range of parameters of the unit cell.

Beam theories based on the Bernoulli–Euler model have been applied to evaluating the macroscopic properties of lattice struts, allowing to predict some of the properties without virtual tests [12]. The analytical description of the mechanical behaviour of unit cells using the Timoshenko beam theory is presented in [13]. However, the applicability of these approaches is strongly limited to regular cells of relatively simple shape represented in the beam formulation.

An important point in the study of additively manufactured metamaterials is the influence of technological processes during their fabrication. In particular, a significant decrease in the mechanical strength was detected for samples built diagonally with respect to the printing direction, accompanied by transformation of the material microstructure during heat treatment [14].

A notable trend in research is to determine the effective distribution of topological parameters of a metamaterial over the volume of a product. In this case, the focus shifts from the search for the optimal shape and size of the unit cell to the search for the optimal distribution of the physical and mechanical parameters within the product to achieve their smooth spatial variation [15]. This approach allows to tailor certain areas of the product to the given operating conditions and control the macroscopic properties of the material depending on the internal forces in a particular area of the structure [16].

A separate extremely interesting class is represented by metamaterials with negative effective Poisson's ratio, the so-called auxetics [17]. According to [18], unit cells capable of generating the auxetic effect are divided into three main groups based on the mechanism underlying that effect: re-entrant cells, chiral cells, and rotating cells. Importantly, the first group is the most promising from the standpoint of manufacturing technologies, including additive manufacturing, since the cells of the second group have a more complex structure, and the cells of the third group comprise structures connected through hinges, so they should be produced by other types of manufacturing technologies. A detailed analysis of the approaches to design of cell struts for auxetic metamaterials and examples of numerical analysis of their mechanical behaviour are given in [19].

As evident from the reviewed literature, interest in metamaterials has been growing steadily over the recent years, and the directions of research are diverse. While there are multiple approaches to studying the mechanical characteristics in this type of structures, the main issue has not been fully resolved. Building on our previous works on lattice structures [20], in this paper, we adopt homogenization methods to carry out numerical calculations of elastic anisotropic properties of metamaterials formed by different types of unit cells, subsequently analysing the relationship between the metamaterial's elastic moduli and topology parameters.

Materials and Methods

The geometry of metamaterials has a periodic structure similar to conventional metallic materials grains formed by crystal lattices. We focus on metamaterials formed by typical lattice structures in this study, and the research methods are based on composite mechanics, elasticity theory of anisotropic media and computational mechanics.

Theoretical aspects of homogenization. Homogenization is a method for estimating the equivalent macroscopic properties of a homogeneous material in such a way that at the global level they are equivalent to the properties of the heterogeneous metamaterial. Such properties of the metamaterial are called effective properties. The results obtained for one cell can be generalized for the whole material due to its periodic structure.

The stresses and strains averaged over a representative volume element are determined by the following formulas:

$$\langle\sigma_{ij}\rangle = \frac{1}{V}\int_V \sigma_{ij}dV,\ \langle\varepsilon_{ij}\rangle = \frac{1}{V}\int_V \varepsilon_{ij}dV,\ \langle\gamma_{ij}\rangle = \frac{1}{V}\int_V \gamma_{ij}dV, \quad (1)$$

where V is the volume of the RVE.

The stresses and strains averaged over the RVE of the metamaterial as assumed to be a homogeneous orthotropic material are related by the equations of generalized Hooke's law written in terms of the principal axes of material symmetry *X*, *Y* and *Z* of the stress and strain tensors:

$$\begin{aligned}
&E_x\langle\varepsilon_{xx}\rangle = \langle\sigma_{xx}\rangle - \nu_{xy}\langle\sigma_{yy}\rangle - \nu_{xz}\langle\sigma_{zz}\rangle,\\
&E_y\langle\varepsilon_{yy}\rangle = -\nu_{yx}\langle\sigma_{xx}\rangle + \langle\sigma_{yy}\rangle - \nu_{yz}\langle\sigma_{zz}\rangle,\\
&E_z\langle\varepsilon_{zz}\rangle = -\nu_{zx}\langle\sigma_{xx}\rangle - \nu_{zy}\langle\sigma_{yy}\rangle + \langle\sigma_{zz}\rangle, \quad (2)\\
&G_{xy}\langle\gamma_{xy}\rangle = \langle\sigma_{xy}\rangle,\\
&G_{yz}\langle\gamma_{yz}\rangle = \langle\sigma_{yz}\rangle,\\
&G_{xz}\langle\gamma_{xz}\rangle = \langle\sigma_{xz}\rangle,
\end{aligned}$$

here E_x, E_y and E_z are the effective Young's moduli of the unit cell; ν_{xy}, ν_{yx}, ν_{yz}, ν_{zy}, ν_{xz} and ν_{zx} are the effective Poisson's ratios; G_{xy}, G_{yz} and G_{xz} are the effective shear moduli.

The expressions of the effective Poisson's ratios can be formulated as follows:

$$\nu_{xy} = \frac{\langle\varepsilon_{yy}\rangle}{\langle\varepsilon_{xx}\rangle},\ \nu_{yx} = \frac{\langle\varepsilon_{xx}\rangle}{\langle\varepsilon_{yy}\rangle},\ \nu_{yz} = \frac{\langle\varepsilon_{zz}\rangle}{\langle\varepsilon_{yy}\rangle},\ \nu_{zy} = \frac{\langle\varepsilon_{yy}\rangle}{\langle\varepsilon_{zz}\rangle},\ \nu_{zx} = \frac{\langle\varepsilon_{xx}\rangle}{\langle\varepsilon_{zz}\rangle},\ \nu_{xz} = \frac{\langle\varepsilon_{zz}\rangle}{\langle\varepsilon_{xx}\rangle}. \quad (3)$$

According to the properties of orthotropic material models, only nine of the twelve material constants are independent, since there are three additional relationships between Poisson's ratios and Young's moduli:

$$E_x\nu_{yx} = E_y\nu_{xy},\ E_y\nu_{zy} = E_z\nu_{yz},\ E_z\nu_{xz} = E_x\nu_{zx}. \quad (4)$$

The compliance matrix [C] relating strains and stresses is based on material constants E_x, E_y, E_z, G_{xy}, G_{yz}, G_{xz}, ν_{xy}, ν_{yz} and ν_{xz} and has the form:

$$[C] = \begin{pmatrix} \frac{1}{E_x} & -\frac{\nu_{yx}}{E_y} & -\frac{\nu_{zx}}{E_z} & 0 & 0 & 0 \\ -\frac{\nu_{xy}}{E_x} & \frac{1}{E_y} & -\frac{\nu_{zy}}{E_z} & 0 & 0 & 0 \\ -\frac{\nu_{xz}}{E_x} & -\frac{\nu_{yz}}{E_y} & \frac{1}{E_z} & 0 & 0 & 0 \\ 0 & 0 & 0 & \frac{1}{G_{xy}} & 0 & 0 \\ 0 & 0 & 0 & 0 & \frac{1}{G_{yz}} & 0 \\ 0 & 0 & 0 & 0 & 0 & \frac{1}{G_{xz}} \end{pmatrix}. \quad (5)$$

In addition to form (2), Hooke's law can be written in the form, which is more common for continuum mechanics as an expression of stress through strain:

$$\begin{pmatrix} \langle\sigma_{xx}\rangle \\ \langle\sigma_{yy}\rangle \\ \langle\sigma_{zz}\rangle \\ \langle\sigma_{xy}\rangle \\ \langle\sigma_{yz}\rangle \\ \langle\sigma_{xz}\rangle \end{pmatrix} = \begin{pmatrix} D_{11} & D_{12} & D_{13} & 0 & 0 & 0 \\ D_{21} & D_{22} & D_{23} & 0 & 0 & 0 \\ D_{31} & D_{32} & D_{33} & 0 & 0 & 0 \\ 0 & 0 & 0 & D_{44} & 0 & 0 \\ 0 & 0 & 0 & 0 & D_{55} & 0 \\ 0 & 0 & 0 & 0 & 0 & D_{66} \end{pmatrix} \cdot \begin{pmatrix} \langle\varepsilon_{xx}\rangle \\ \langle\varepsilon_{yy}\rangle \\ \langle\varepsilon_{zz}\rangle \\ \langle\gamma_{xy}\rangle \\ \langle\gamma_{yz}\rangle \\ \langle\gamma_{xz}\rangle \end{pmatrix}, \quad (6)$$

where $[D]$ is the stiffness matrix that corresponds to the 4[th]-rank tensor of elastic moduli and is the inverse of the compliance matrix:

$$[D] = [C]^{-1}. \quad (7)$$

Six numerical tests are required to determine the independent constants: three uniaxial tension tests and three shear tests. When each test is considered separately, relation (6) takes a simplified form, where $\langle\sigma_{ij}^x\rangle$, $\langle\sigma_{ij}^y\rangle$ and $\langle\sigma_{ij}^z\rangle$ are the stresses in uniaxial tensile tests along axes *X*, *Y* and *Z* respectively, $\langle\sigma_{ij}^{xy}\rangle$, $\langle\sigma_{ij}^{yz}\rangle$ and $\langle\sigma_{ij}^{xz}\rangle$ are the stresses in the shear tests in planes *XY*, *YZ* and *ZX* respectively (here $i, j \in \{x, y, z\}$):

$$A\begin{pmatrix} D_{11} \\ D_{21} \\ D_{31} \\ 0 \\ 0 \\ 0 \end{pmatrix} = \begin{pmatrix} \langle\sigma_{xx}^x\rangle \\ \langle\sigma_{yy}^x\rangle \\ \langle\sigma_{zz}^x\rangle \\ 0 \\ 0 \\ 0 \end{pmatrix}, A\begin{pmatrix} D_{12} \\ D_{22} \\ D_{32} \\ 0 \\ 0 \\ 0 \end{pmatrix} = \begin{pmatrix} \langle\sigma_{xx}^y\rangle \\ \langle\sigma_{yy}^y\rangle \\ \langle\sigma_{zz}^y\rangle \\ 0 \\ 0 \\ 0 \end{pmatrix}, A\begin{pmatrix} D_{13} \\ D_{23} \\ D_{33} \\ 0 \\ 0 \\ 0 \end{pmatrix} = \begin{pmatrix} \langle\sigma_{xx}^z\rangle \\ \langle\sigma_{yy}^z\rangle \\ \langle\sigma_{zz}^z\rangle \\ 0 \\ 0 \\ 0 \end{pmatrix}, \quad (8)$$

$$A\begin{pmatrix} 0 \\ 0 \\ 0 \\ D_{44} \\ 0 \\ 0 \end{pmatrix} = \begin{pmatrix} 0 \\ 0 \\ 0 \\ \langle\sigma_{xy}^{xy}\rangle \\ 0 \\ 0 \end{pmatrix}, A\begin{pmatrix} 0 \\ 0 \\ 0 \\ 0 \\ D_{55} \\ 0 \end{pmatrix} = \begin{pmatrix} 0 \\ 0 \\ 0 \\ 0 \\ \langle\sigma_{yz}^{yz}\rangle \\ 0 \end{pmatrix}, A\begin{pmatrix} 0 \\ 0 \\ 0 \\ 0 \\ 0 \\ D_{66} \end{pmatrix} = \begin{pmatrix} 0 \\ 0 \\ 0 \\ 0 \\ 0 \\ \langle\sigma_{xz}^{xz}\rangle \end{pmatrix}, \quad (9)$$

where *A* is the value of longitudinal strain along one of the principal orthotropy axes or under shear in one of the principal orthotropy planes. The value of *A* here and below is taken equal to 0.001.

The averaged stresses during numerical homogenization are taken as the ratio of the force F_k, arising under deformation of the unit cell and applied to its face, to the area of this face S:

$$\langle \sigma_{ij}^k \rangle = \frac{F_k}{S}, \tag{10}$$

where $i, j \in \{x, y, z\}$, $k \in \{x, y, z, xy, yz, xz\}$.

The index k in formula (10) corresponds to the test conducted: x is the tension along the X axis, y is the tension along the Y axis, z is the tension along the Z axis, xy is the shear in the XY plane, yz is the shear in the YZ plane, xz is the shear in the XZ plane.

The unknown components of the stiffness matrix D_{ij} can be obtained based on the results of the six tests:

$$[D] = \begin{pmatrix} D_{11} & D_{12} & D_{13} & 0 & 0 & 0 \\ D_{21} & D_{22} & D_{23} & 0 & 0 & 0 \\ D_{31} & D_{32} & D_{33} & 0 & 0 & 0 \\ 0 & 0 & 0 & D_{44} & 0 & 0 \\ 0 & 0 & 0 & 0 & D_{55} & 0 \\ 0 & 0 & 0 & 0 & 0 & D_{66} \end{pmatrix}. \tag{11}$$

Next, the compliance matrix components can be found in accordance with Eq. (7). After that, all unknown elastic constants can be found from Eq. (5):

$$\begin{gathered} E_x = \frac{1}{c_{11}}, E_y = \frac{1}{c_{22}}, E_z = \frac{1}{c_{33}}, \\ G_{xy} = \frac{1}{c_{44}}, G_{yz} = \frac{1}{c_{55}}, G_{xz} = \frac{1}{c_{66}}, \\ \nu_{xy} = -\frac{c_{21}}{c_{11}}, \nu_{xz} = -\frac{c_{31}}{c_{11}}, \nu_{yz} = -\frac{c_{32}}{c_{22}}. \end{gathered} \tag{12}$$

Because the metamaterial is a periodic structure, numerical experiments should be performed with boundary conditions different from the traditional ones. Periodic boundary conditions adequately describe the three-dimensional symmetry of the structure, also providing a more physical deformation of the material, since they reflect the direct mutual influence of deformation of the given cell on its neighbouring cells.

The periodic boundary conditions show the same displacements of each pair of nodes on opposite faces of the unit cell of size $L_x \times L_y \times L_z$. Three tensile tests and three shear tests were conducted to determine the material parameters under the boundary conditions described above.

The following periodic boundary conditions have to be satisfied on pairs of opposite sides of the RVE, respectively, to perform three numerical uniaxial tensile tests sequentially along the X, Y, and Z axes.

Tension along the X axis:

$$\mathbf{u}|_{x=0} - \mathbf{u}|_{x=L_x} = A\mathbf{i}, \mathbf{u}|_{y=0} - \mathbf{u}|_{y=L_y} = 0, \mathbf{u}|_{z=0} - \mathbf{u}|_{z=L_z} = 0. \tag{13}$$

Tension along the Y axis:

$$\mathbf{u}|_{x=0} - \mathbf{u}|_{x=L_x} = 0, \mathbf{u}|_{y=0} - \mathbf{u}|_{y=L_y} = A\mathbf{j}, \mathbf{u}|_{z=0} - \mathbf{u}|_{z=L_z} = 0. \tag{14}$$

Tension along the Z axis:

$$\mathbf{u}|_{x=0} - \mathbf{u}|_{x=L_x} = 0, \mathbf{u}|_{y=0} - \mathbf{u}|_{y=L_y} = 0, \mathbf{u}|_{z=0} - \mathbf{u}|_{z=L_z} = A\mathbf{k}. \tag{15}$$

where $\mathbf{u}$ is the displacement vector of RVE points; **i, j** and $\mathbf{k}$ are the coordinate system basis vectors along axes X, Y and Z.

The following periodic boundary conditions have to be satisfied on pairs of opposite sides of the RVE to perform three shear tests sequentially in the XY, YZ and XZ planes.

Shear in the XY plane:

$$\mathbf{u}|_{x=0} - \mathbf{u}|_{x=L_x} = A\mathbf{j}, \mathbf{u}|_{y=0} - \mathbf{u}|_{y=L_y} = A\mathbf{i}, \mathbf{u}|_{z=0} - \mathbf{u}|_{z=L_z} = 0. \tag{16}$$

Shear in the YZ plane:

$$\mathbf{u}|_{x=0} - \mathbf{u}|_{x=L_x} = 0, \mathbf{u}|_{y=0} - \mathbf{u}|_{y=L_y} = A\mathbf{k}, \mathbf{u}|_{z=0} - \mathbf{u}|_{z=L_z} = A\mathbf{j}. \tag{17}$$

Shear in the *XZ* plane:

$$\mathbf{u}|_{x=0} - \mathbf{u}|_{x=L_x} = A\mathbf{k}, \mathbf{u}|_{y=0} - \mathbf{u}|_{y=L_y} = 0, \mathbf{u}|_{z=0} - \mathbf{u}|_{z=L_z} = A\mathbf{i}. \quad (18)$$

Estimation of elastic properties of metamaterial in non-principal axes. Changing the direction of the local axes of the unit cell allows estimating the characteristics of the metamaterial in a different direction, which can have a positive effect on changing the parameters of the unit cell and the metamaterial as a whole. Specifically, the values of the elastic characteristics of the unit cell may turn out to be higher along the rotated axes, making it possible to arrange the lattice structure more rationally within the designed product and render it more resistant to applied loads. This section considers the behaviour of lattice properties when local axes of the unit cell are rotated relative to the initial orientation of the metamaterial axes (Fig. 1).

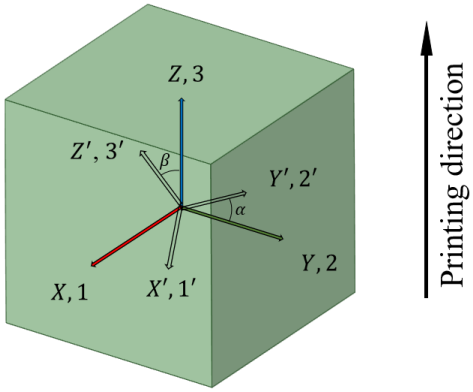

Fig. 1. Axis layout and printing direction

We "rotate" the stiffness matrix in the equation, corresponding to the 4th-rank elastic moduli tensor. The deformation directions remain unchanged.

The combination of two rotations around three orthogonal vectors *X*, *Y*, *Z* is taken as the rotation tensor. However, it does not seem possible to rotate a 6 × 6 matrix by a 3 × 3 rotation matrix. Instead, the 4th-rank tensor must be recovered for this purpose from the 6×6 matrix by the Voigt notation rule explained below:

$$\begin{pmatrix} C_{11} \to C_{1111} & C_{12} \to C_{1122} & C_{13} \to C_{1133} & C_{14} \to C_{1123} & C_{15} \to C_{1131} & C_{16} \to C_{1112} \\ C_{21} \to C_{2211} & C_{22} \to C_{2222} & C_{23} \to C_{2233} & C_{24} \to C_{2223} & C_{24} \to C_{2231} & C_{26} \to C_{2212} \\ C_{31} \to C_{3311} & C_{32} \to C_{3322} & C_{33} \to C_{3333} & C_{34} \to C_{3323} & C_{35} \to C_{3331} & C_{36} \to C_{3312} \\ C_{41} \to C_{2311} & C_{42} \to C_{2322} & C_{43} \to C_{2333} & C_{44} \to C_{2323} & C_{45} \to C_{2331} & C_{46} \to C_{2312} \\ C_{51} \to C_{3111} & C_{52} \to C_{3122} & C_{53} \to C_{3133} & C_{54} \to C_{3123} & C_{55} \to C_{3131} & C_{56} \to C_{3112} \\ C_{61} \to C_{1211} & C_{62} \to C_{1222} & C_{63} \to C_{1233} & C_{64} \to C_{1223} & C_{65} \to C_{1231} & C_{66} \to C_{1212} \end{pmatrix} \quad (19)$$

The 4th-rank elastic moduli tensor C_{ijkl} is symmetric with respect to the first and second pairs of indices:

$$C_{ijkl} = C_{jikl} = C_{ijlk}. \quad (20)$$

The elements can be written as a 6×6 matrix using the following index substitution:

$$11 \to 1; 22 \to 2; 33 \to 3; 23, 32 \to 4; 13, 31 \to 5; 12, 21 \to 6. \quad (21)$$

As one Cartesian coordinate system x_1, x_2, x_3 is converted to another Cartesian coordinate system x_1', x_2', x_3', the components of the elastic moduli tensor are transformed as follows (the Einstein notation for summation over repeated indices is used here):

$$C'_{ijkl} = n_{i\alpha}n_{j\beta}n_{k\gamma}n_{l\delta}C_{\alpha\beta\gamma\delta}, \quad (22)$$

where n_{mn} are the directional cosines between the *m*, *n* axes, which can be determined from the formula:

$$n_{mn} = \frac{x_m \cdot x_n}{|x_m||x_n|}. \quad (23)$$

In our case, the axes are rotated by the angle α lying in the range from 0 to 2π with the step 0.02π around the Z axis and by the angle β in the range from $-\pi/2$ to $\pi/2$ with the step 0.01π in the case of rotation around the rotated Y axis. The rotation matrices are constructed by the angles given at each step:

$$P_z = \begin{pmatrix} cos\alpha & -sin\alpha & 0 \\ sin\alpha & cos\alpha & 0 \\ 0 & 0 & 1 \end{pmatrix}, \quad (24)$$

$$P_y = \begin{pmatrix} cos\beta & 0 & sin\beta \\ 0 & 1 & 0 \\ -sin\beta & 0 & cos\beta \end{pmatrix}. \quad (25)$$

Thus, the rotated axes can be calculated by the formula:

$$x_i' = P_y \cdot P_z \cdot x_i,\ i \in \{1, 2, 3\}. \quad (26)$$

The matrix of elastic moduli C'_{ijkl} is calculated from Eq. (22) in the local (rotated) coordinate system. After that, the values of elastic constants in the rotated coordinate system can be obtained by Eq. (12).

Calculating the moduli values for each of the specified angle values, we obtain a circular diagram reflecting the dependence of the considered mechanical characteristics on the direction of local axes. For convenience, matrix transformations, orthogonal rotation and other related calculations are performed with the code in MATLAB package. Such transformations were performed for each type of unit cell.

Geometric models for unit cells of the metamaterial. Geometric models of unit cells of the metamaterial are designed assuming that the basic cells can be formed by rods of different diameters and have different volume fractions of solid material. SolidWorks computer-aided design system was used to build the geometric models [21].

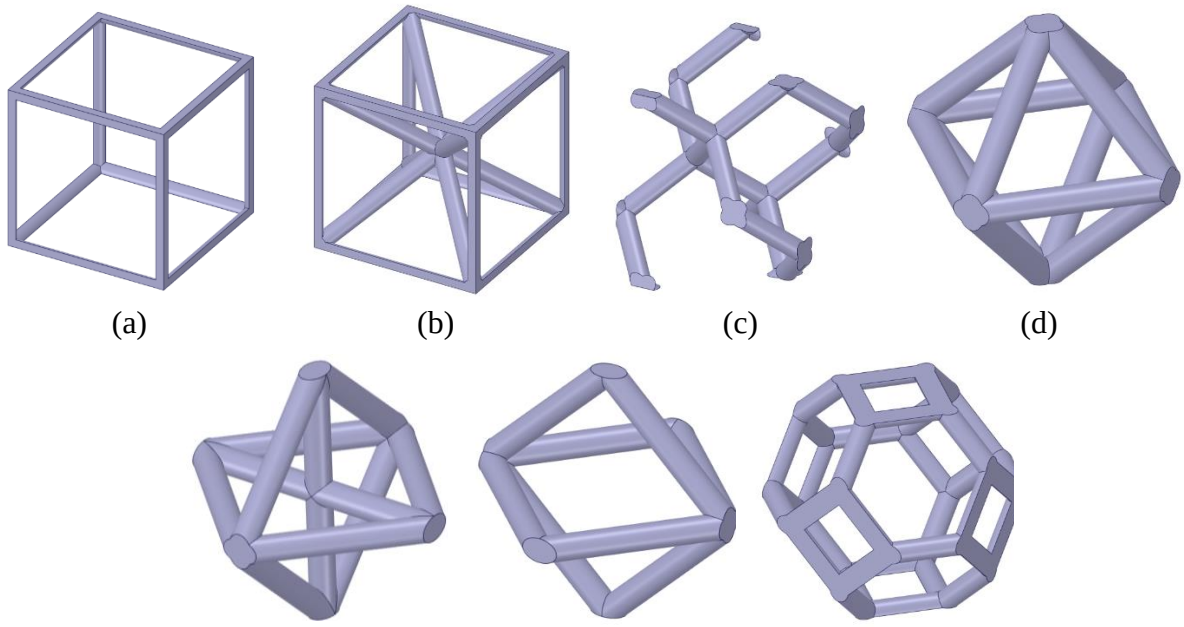

Fig. 2. Unit cells of metamaterials: (a) cell of type 1, (b) cell of type 2, (c) cell of type 3, (d) cell of type 4, (e) cell of type 5, (f) cell of type 6, (g) cell of type 7

Each cell type has the overall dimensions of 10 × 10 × 10 mm. The 3D view of the designed unit cells is shown in Fig. 2. The topology of the cells was chosen as the most interesting and promising for further research. The designs presented in Fig. 2 are based on a single rod 1.0 mm in diameter.

Several modifications of the structure geometry are adopted to comprehensively analyse the influence of the metamaterial unit cell topology, as well as to correctly compare the lattices with each other.

We primarily focus on the effect of the volume fraction of the lattice structure material and the effect of the ratio of the unit cell dimensions L_x, L_y and L_z on the macroscopic properties of the metamaterial. The analysis in this section aimed to establish the dependence of the macroscopic properties of the metamaterial on its effective density for each of the seven cell types considered.

Several modifications of the structure geometry are adopted to comprehensively analyse the influence of the metamaterial unit cell topology, as well as to correctly compare the lattices with each other.

We primarily focus on the effect of the volume fraction of the lattice structure material and the effect of the ratio of the unit cell dimensions L_x, L_y and L_z on the macroscopic properties of the metamaterial. The analysis in this section aimed to establish the dependence of the macroscopic properties of the metamaterial on its effective density for each of the seven cell types considered.

The effective density of metamaterial is understood as the ratio of the volume of solid material contained in a unit cell to the volume of a parallelepiped with the characteristic size $L_x \times L_y \times L_z$. The volume fraction varies from 0.01 to 1, where 1 corresponds to solid material. The mechanical characteristics were calculated by taking 10 points in the range from 0.01 to 0.1, and then another 24 points with a constant step of 0.0375. Figures 3–9 show the geometric shapes for each of the cell types for the four volume fractions of the material.

Cells with the characteristic size $L_x = L_y = L_z = 10$ mm are considered above. Departing from the traditional understanding of a cubic unit cell, we introduce a range of variation for one of the geometrical parameters, the value of length L_x. Let us estimate the variation trends of the metamaterial parameters with varying ratio of unit cell sizes. The value of length L_x varies from 10 to 1 mm with the step of 1 mm for each cell under consideration.

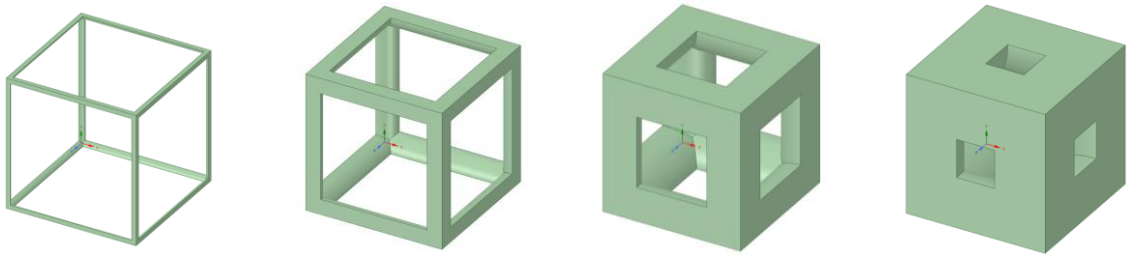

(a) (b) (c) (d)

Fig. 3. Unit cell of type 1 with different volume fractions of the material: (a) 0.01; (b) 0.1; (c) 0.4; (d) 0.7

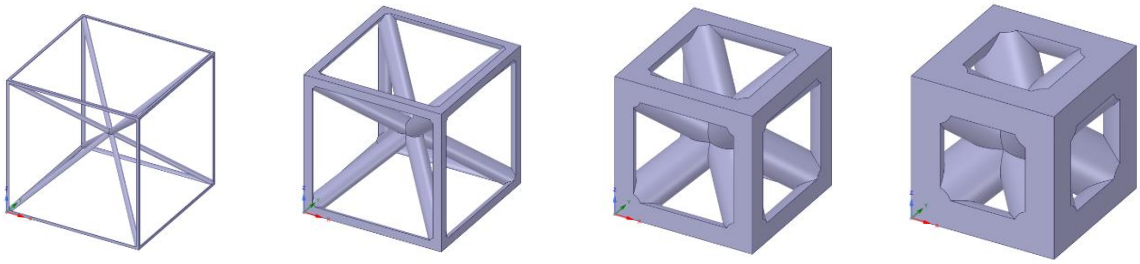

(a) (b) (c) (d)

Fig. 4. Unit cell of type 2 with different volume fractions of the material: (a) 0.01; (b) 0.1; (c) 0.4; (d) 0.7

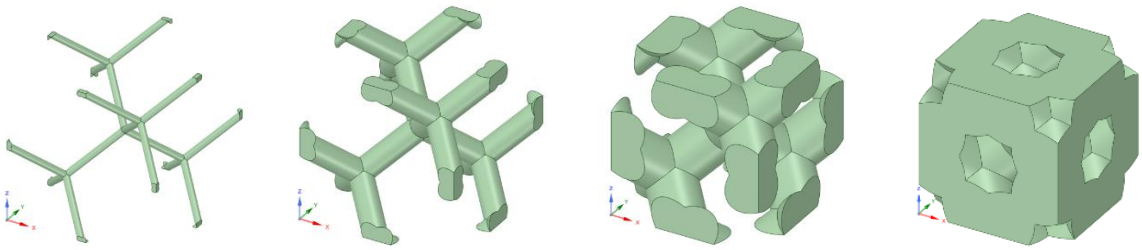

(a) (b) (c) (d)

Fig. 5. Unit cell of type 3 with different volume fractions of the material: (a) 0.01; (b) 0.1; (c) 0.4; (d) 0.7

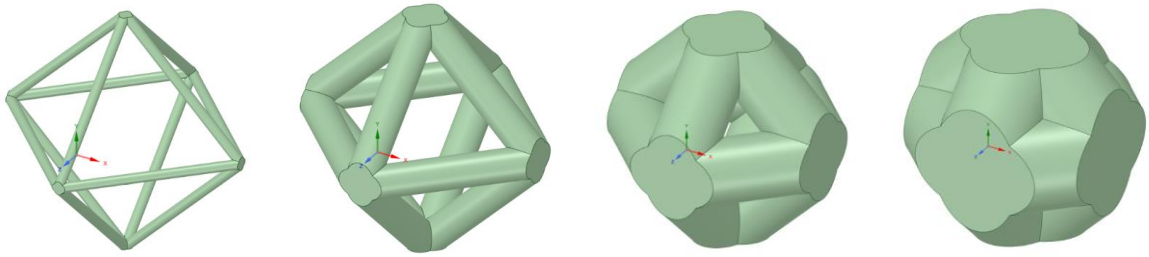

(a) (b) (c) (d)

Fig. 6. Unit cell of type 4 with different volume fractions of the material: (a) 0.01; (b) 0.1; (c) 0.4; (d) 0.7

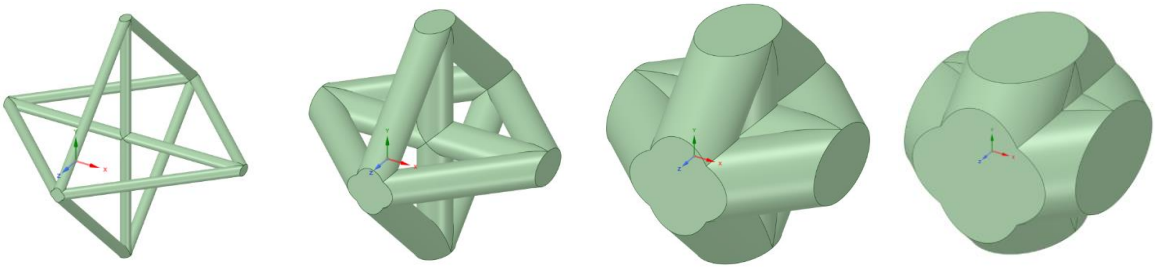

(a) (b) (c) (d)

Fig. 7. Unit cell of type 5 with different volume fractions of the material: (a) 0.01; (b) 0.1; (c) 0.4; (d) 0.7

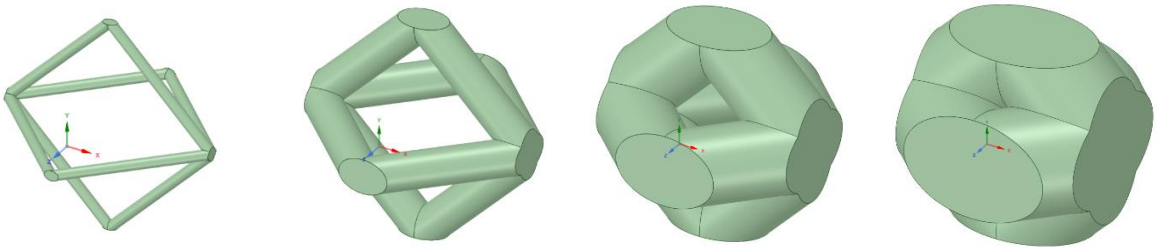

(a) (b) (c) (d)

Fig. 8. Unit cell of type 6 with different volume fractions of the material: (a) 0.01; (b) 0.1; (c) 0.4; (d) 0.7

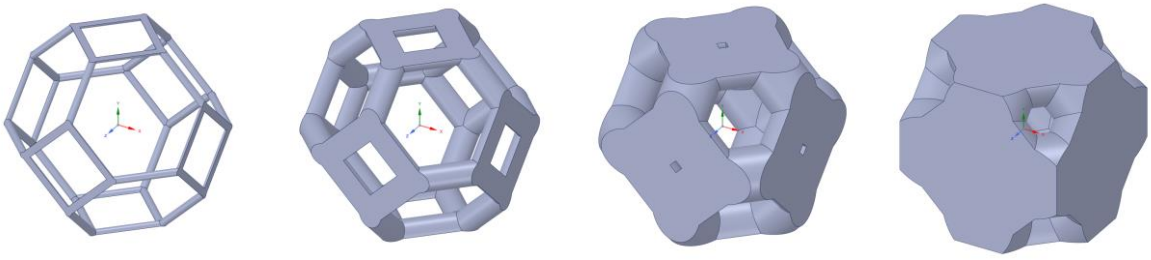

(a) (b) (c) (d)

Fig. 9. Unit cell of type 7 with different volume fractions of the material: (a) 0.01; (b) 0.1; (c) 0.4; (d) 0.7

Figures 10–16 show the 3D view for four topologies of each type of unit cells with $L_x \in \{10, 7, 4, 1\}$. For correct analysis of the results, homogenization was performed at a fixed volume fraction of 0.05.

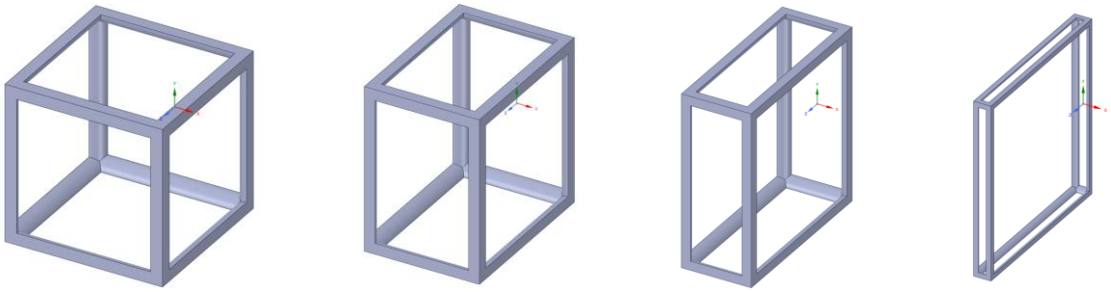

(a) (b) (c) (d)

Fig. 10. Unit cell of type 1 with varying dimension L_x: (a) 10 mm, (b) 7 mm, (c) 4 mm, (d) 1 mm

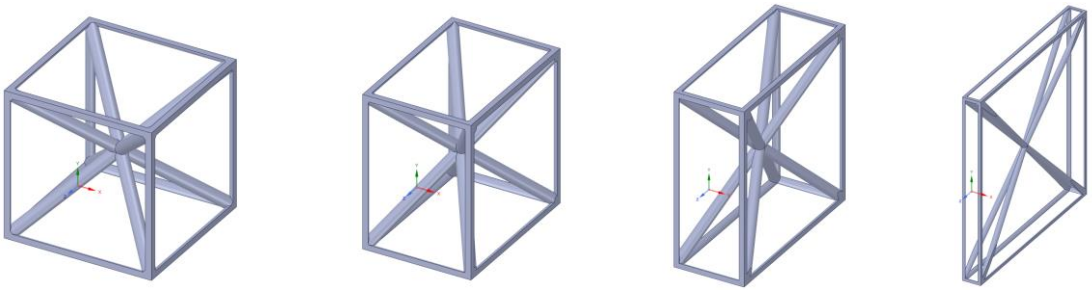

(a) (b) (c) (d)

Fig. 11. Unit cell of type 1 with varying dimension L_x: (a) 10 mm, (b) 7 mm, (c) 4 mm, (d) 1 mm

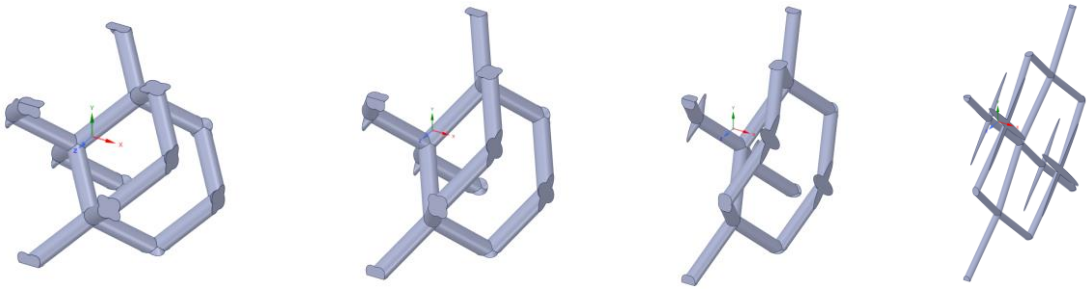

(a) (b) (c) (d)

Fig. 12. Unit cell of type 1 with varying dimension L_x: (a) 10 mm, (b) 7 mm, (c) 4 mm, (d) 1 mm

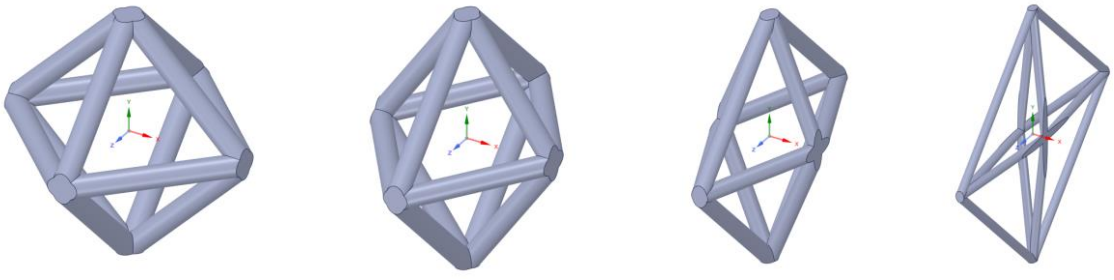

(a) (b) (c) (d)

Fig. 13. Unit cell of type 1 with varying dimension L_x: (a) 10 mm, (b) 7 mm, (c) 4 mm, (d) 1 mm

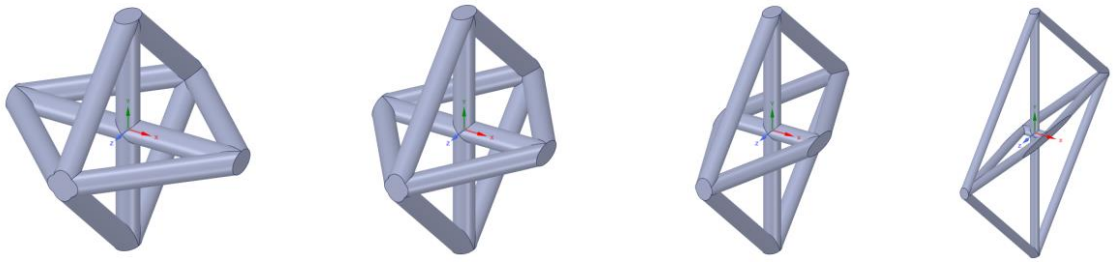

(a) (b) (c) (d)

Fig. 14. Unit cell of type 1 with varying dimension L_x: (a) 10 mm, (b) 7 mm, (c) 4 mm, (d) 1 mm

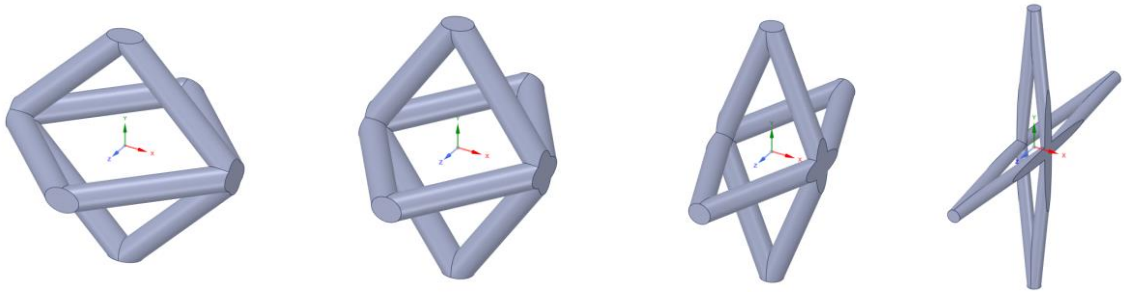

(a) (b) (c) (d)

Fig. 15. Unit cell of type 1 with varying dimension L_x: (a) 10 mm, (b) 7 mm, (c) 4 mm, (d) 1 mm

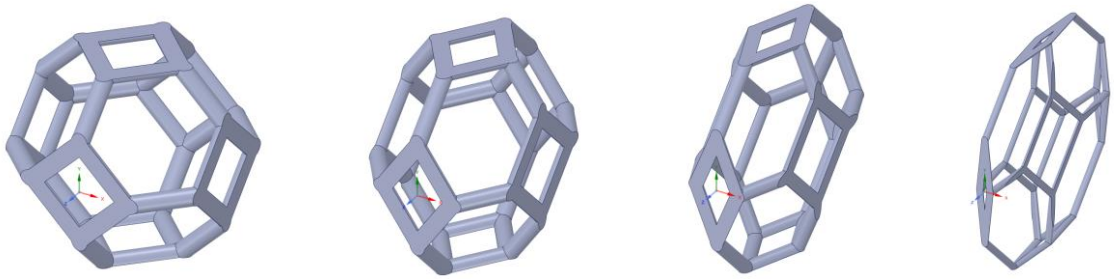

(a) (b) (c) (d)

Fig. 16. Unit cell of type 1 with varying dimension L_x: (a) 10 mm, (b) 7 mm, (c) 4 mm, (d) 1 mm

Finite element models of metamaterial unit cells. A series of finite element models were developed based on the presented three-dimensional geometric models (Figs. 3–16). The models are formed by tetrahedral finite elements with first-order displacement interpolation. The classical finite element method in displacements with variational formulation based on the weighted residuals method or the principle of minimum potential energy is used for the three-dimensional problem of elasticity theory [22].

The homogenization process for the metamaterial is carried out according to the algorithm described above using the finite element analysis system ANSYS Material Designer. The characteristic problems of elasticity theory are solved in a static formulation using the considered periodic boundary conditions (13)–(18).

The computational domain of each type of metamaterial represents one unit cell. The maximum size of the finite element of the computational mesh is 1 mm. The characteristic mesh size depends on the thickness of the rod forming the unit cell, covering the range from 0.005 to 1 mm and selected for each cell type individually taking into account the volume fraction of the solid material.

Typical examples of finite element meshes are shown in Figs. 17 and 18. The numbers of elements and nodes in the numerical models are given in Table 1 for unit cells of types 1–7 with 0.4 vol. % of the material as a typical example.

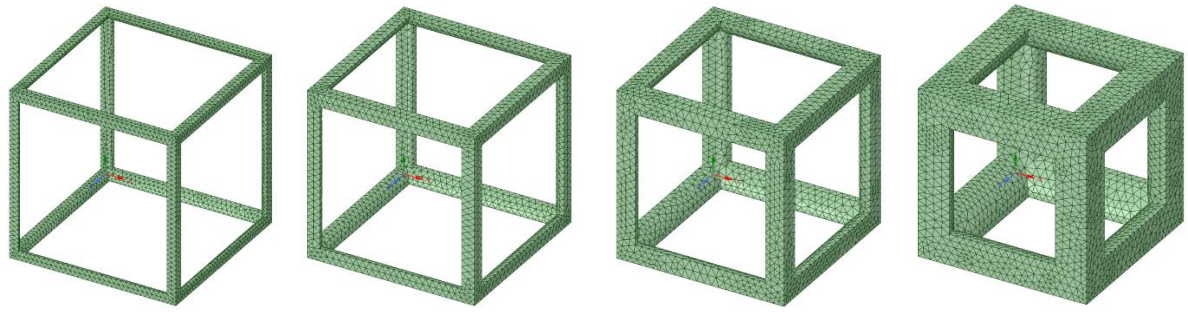

(a) (b) © (d)

Fig. 17. Finite element mesh for unit cells of type 1 with different volume fractions of the material: (a) volume fraction 0.025, mesh size 0.3 mm, (b) volume fraction 0.05, mesh size 0.4 mm, (c) volume fraction 0.1, mesh size 0.45 mm, (d) volume fraction 0.25, mesh size 0.5 mm

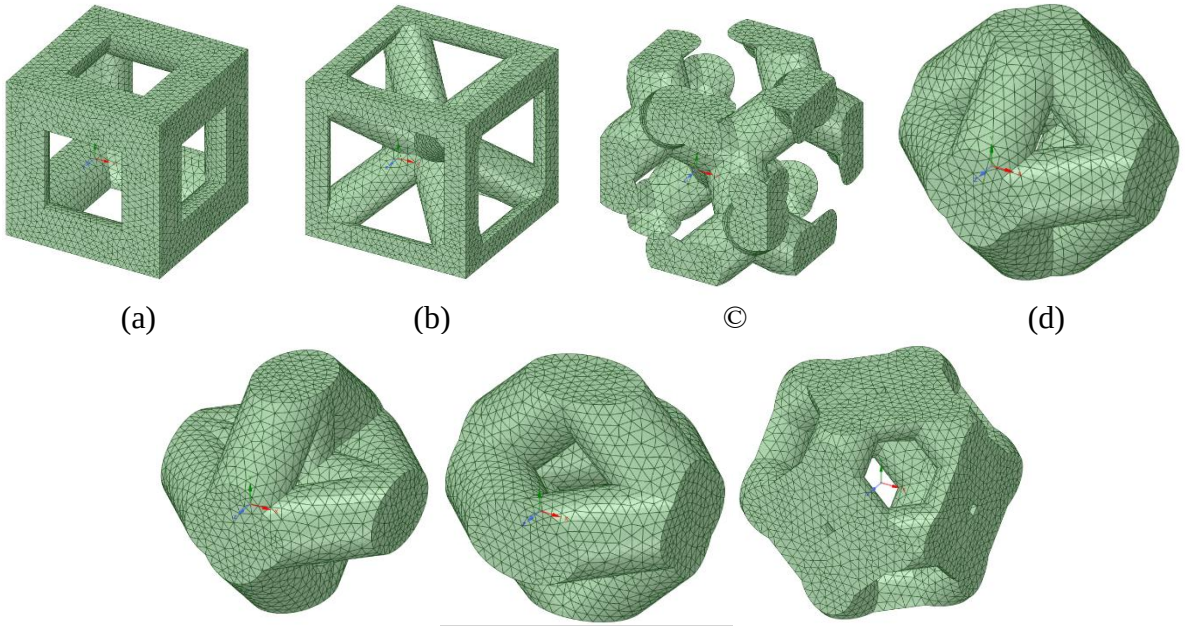

(a) (b) © (d)

© (f) (g)

Fig. 18. Finite element mesh for unit cells of types 1–7 with 0.4 vol.% of the material: (a) type 1, (b) type 2, (c) type 3, (d) type 4, (c) type 5, (f) type 6, (g) type 7

Table 1. Mesh statistics for finite element models of unit cells with 0.4 vol. % of the material

Unit cell type	Number of elements	Number of nodes
1	40 743	63 706
2	37 920	59 799
3	32 162	50 098
4	28 606	42 551
5	30 609	45 272
6	30 245	44 863
7	33 133	51 415

Representative elements are considered to check the adequacy and correctness of the introduced periodic boundary conditions (13)–(18). Provided that the elasticity theory problem is well-posed for a periodic composite material with periodic boundary conditions, the homogenization problem can be solved numerically for a representative volume element consisting of $1 \times 1 \times 1$ basic or unit cells. However, it is certainly possible to study the

behaviour of the RVEs consisting of 3 × 3 × 3 and 5 × 5 × 5 unit cells, since they can be considered as the representative volume elements of larger size (Fig. 19).

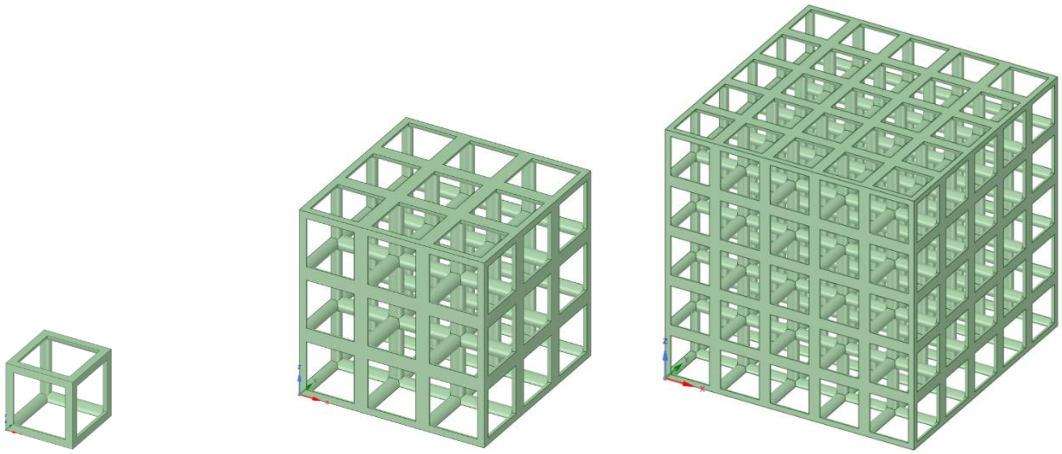

(a) (b) ©

Fig. 19. Representative volume elements with different numbers of unit cells: (c) 1 × 1 ×1 unit cells, (b) 3 × 3 × 3 unit cells, (c) 5 × 5 × 5 unit cells

This step is necessary for checking whether the periodic boundary conditions adopted are well-posed and the overall methodology is sound. Because the RVE is large-sized, a larger number of finite elements have to be processed (Table 2), which significantly increases the computational cost of the research. Therefore, it seems reasonable to assess the influence of the number of unit cells in the RVE on the values of the obtained elastic characteristics of the metamaterial.

Table 2. Mesh statistics for finite element models of representative volume elements formed by different numbers of unit cells

Number of unit cells in RVE	Number of elements	Number of nodes
1 × 1 × 1	5 450	10 533
3 × 3 × 3	119 466	208 914
5 × 5 × 5	574 758	980 132

Mechanical properties of the material. Finally, to formulate the problem of elasticity theory for the case of additively manufactured materials, we should tailor the mechanical properties to account for potential anisotropy. Our study considers the metamaterials produced additively from $AlSi_{10}Mg$ by selective laser melting (SLM) with the powder particle size less than 150 μm. The material and the technique can be used to produce parts with thin structural elements and complex geometry, also well suited for manufacturing of lightweight products.

Table 3. Mechanical properties of additively manufactured $AlSi_{10}Mg$ alloy

Mechanical property type	Direction		
	X/XY	Y/YZ	Z/XZ
Young's modulus, Gpa	82.5	76.7	76.8
Shear modulus, Gpa	23.8	27.1	21.4
Poisson's ratio	0.32	0.32	0.33

The values of technical elastic properties of the solid material obtained by selective melting 0 are given in Table 3. The orientation of coordinate system axes and printing direction are shown in Fig. 1. As seen from Table 3, adopting the SLM technology for producing

metamaterials yields a slightly pronounced orthotropy of the properties, which is taken into account when selecting a non-isotropic model of the material for numerical analysis.

Results and Discussion

This section presents the computational results for the elastic properties of metamaterials of all types with varying volume fraction of solid material within the unit cell. We also carried out an analysis of Young's moduli values depending on the rotation of the local axes relative to the principal axes of material symmetry, as well as analysis of the effect of compression of the unit cell shape along one of the coordinate axes.

Verification of boundary conditions. To verify the adequacy and correctness of the mathematical formulation of the problem and periodic boundary conditions imposed on pairs of nodes of the mesh, the effective mechanical properties of the structures consisting of $1 \times 1 \times 1$, $3 \times 3 \times 3$ and $5 \times 5 \times 5$ unit cells of type 1 were evaluated (Fig. 19). The volume fraction of the material of the analysed cells was taken equal to 0.1. In our opinion, verifying only one type of metamaterial should be sufficient to draw the required conclusions, since the results for the rest of the cells should be similar due to the uniformity of the used algorithm. The computations are performed on an Intel Core i7 CPU (10^{th} generation) workstation with 64 Gb DDR4 RAM. The duration of analysis for the models with $1 \times 1 \times 1$, $3 \times 3 \times 3$ and $5 \times 5 \times 5$ cells was 40, 181 and 810 seconds, respectively.

The computational results for the three cases of the metamaterial RVE are presented in Table 4. The relative differences are given in the table compared to the $5 \times 5 \times 5$ structure.

Table 4. Young's moduli for different numbers of unit cells in representative volumes of type 1 metamaterial

Mechanical property type	RVE with $1 \times 1 \times 1$ unit cells	RVE with $3 \times 3 \times 3$ unit cells	RVE with $5 \times 5 \times 5$ unit cells
E_1, Mpa	3 366.2	3 366.1	3 366.4
E_2, Mpa	3 137.8	3 137.9	3 138.2
E_3, Mpa	3 140.2	3 140.6	3 140.9
Relative difference for E_1, %	0.006	0.009	–
Relative difference for E_2, %	0.013	0.010	–
Relative difference for E_3, %	0.022	0.009	–

As seen from Table 4, the relative differences in Young's moduli between the three RVEs is less than 0.03 %, which is within the numerical errors of finite element analysis. At the same time, the computations for the RVE consisting of $5 \times 5 \times 5$ unit cells take more than 15 times longer compared to the computations for the RVE with $1 \times 1 \times 1$ unit cells.

Thus, it is safe to assume that the mathematical model is correct and subsequent computations can be performed with the periodic boundary conditions (13)–(18) without compromising the accuracy of the results for an RVE consisting of one unit cell with the characteristic size of $10 \times 10 \times 10$ mm.

Results for the case of rods with fixed diameter. The computational time for one metamaterial unit cell is about 3 minutes depending on the geometric complexity. The results of finite element homogenization for unit cells of types 1–7 at fixed diameter of rods are presented in Table 5.

Since the rod diameters of all unit cells of the metamaterials are the same and equal to 1 mm, the volume fraction of the material in each of the unit cells is different (Table 6). This should be taken into account in the comparative analysis of elastic moduli. We can approximately consider Young's and shear moduli to be proportional to the material volume fraction for small values.

Nevertheless, only the simplest structure of type 1 contains a significantly lower volume fraction of the material, while the other cells are filled with the base material by about the same 4.1–6.9 %.

Table 5. Effective elastic moduli of metamaterials with different types of unit cells at fixed rod diameter (1 mm)

Mechanical property type	Unit cell of type 1	Unit cell of type 2	Unit cell of type 3	Unit cell of type 4	Unit cell of type 5	Unit cell of type 6	Unit cell of type 7
E_1, Mpa	665.4	908.2	80.3	594.3	897.3	59.5	231.3
E_2, Mpa	619.3	863.4	78.9	595	854.7	56	240.2
E_3, Mpa	620	863.9	79.5	593.6	595.8	55.6	234.3
G_{12}, Mpa	2.7	422.8	82.9	386.9	5.4	372.2	62.2
G_{23}, Mpa	2.6	428.9	84	421.9	415.4	2.6	62.9
G_{31}, MPa	2.6	417.5	82.2	359.3	352.6	344.9	61.7
ν_{12}	0.03	0.29	0.47	0.33	-0.2	0.9	0.4
ν_{13}	0.03	0.29	0.46	0.28	0.5	0.9	0.4
ν_{23}	0.03	0.29	0.49	0.37	0.6	-0.9	0.4

Table 6. Volume fraction of material for rod diameter of 1 mm

Unit cell type	Unit cell of type 1	Unit cell of type 2	Unit cell of type 3	Unit cell of type 4	Unit cell of type 5	Unit cell of type 6	Unit cell of type 7
Volume fraction	0.022	0.069	0.049	0.059	0.053	0.041	0.059

We can conclude from these preliminary computations that the effective elastic properties of the metamaterial depend significantly on the geometry of the unit cell forming the periodic structure of the metamaterial. Cells of types 1, 2 and 5 exhibit the highest stiffnesses along the principal orthotropy axes. The geometry of these cells contains the rods that are parallel to the loading axes, making the material more resistant to tension–compression.

Cells of types 2 and 4 exhibit the highest shear stiffness, determined by the shear modulus, apparently due to the presence of transverse rods connecting the diagonal nodes of the lattice. Metamaterials based on type 5 and 6 cells also have rather high shear stiffnesses, but only in two planes, which is due to incomplete symmetry of the cells with respect to the coordinate planes.

Metamaterials based on types 3 and 6 cells have the lowest values of Young's and shear moduli along the axes of the global coordinate system. A possible explanation for this is that these cell types are formed mainly by diagonal rods and, therefore, do not have high stiffness in the considered directions. Nevertheless, it can be hypothesized that the properties may be higher in other directions (this point is discussed below).

The simplest cell of type 1 exhibits the highest stiffness along the three principal directions due to its characteristic cubic shape with no additional diagonal rods. However, its shear stiffness as well as its Poisson's ratio are minimal. The significant difference in Young's moduli along the *Z* axis for the cell of type 5 compared to the same parameter along the *X* and *Y* axes is due to the absence of the rod in the unit cell in this direction.

Interestingly, the metamaterials based on cells of types 5 and 6 have auxetic properties, which is confirmed by the negative values of Poisson's ratio in certain planes. Both positive and negative values of Poisson's ratio are rather high for these cell types. Analysing the geometry of these cells, we can assume that diagonally arranged rods lead to the auxetic effect, and the metamaterials themselves can be classified as auxetics based on re-entrant cells.

The computations ultimately confirm that all types of metamaterials exhibit material symmetry of elastic properties with respect to the three orthotropy planes. The structural anisotropy is in this case apparently complemented by the initial non-isotropy of the material properties due to additive manufacturing by selective laser melting.

The volume fraction of the material in the unit cell of the metamaterial can serve as an additional criterion of efficiency along with the elastic properties. We assume that a metamaterial with a lower content of initial material but higher stiffness is more efficient than a metamaterial with similar elastic properties but lower porosity. We should also note that the

presence of a system with branched pore channels in metamaterials can be a crucial factor in some applications, in particular for biomedicine [23].

Effect of material volume fraction on metamaterial properties. Let us start the analysis of the effective properties of the metamaterial formed by different types of cells by considering the comparative graphs illustrating the differences in the variation of Young's moduli, shear moduli, and Poisson's ratio at the same value of the material volume fraction. Figure 20 shows the variations of elastic constants of the metamaterial as functions of porosity. The results are given as curves of the dependences of Young's moduli, shear moduli and Poisson's ratios along the principal axes of orthotropy on the volume fraction of the initial material.

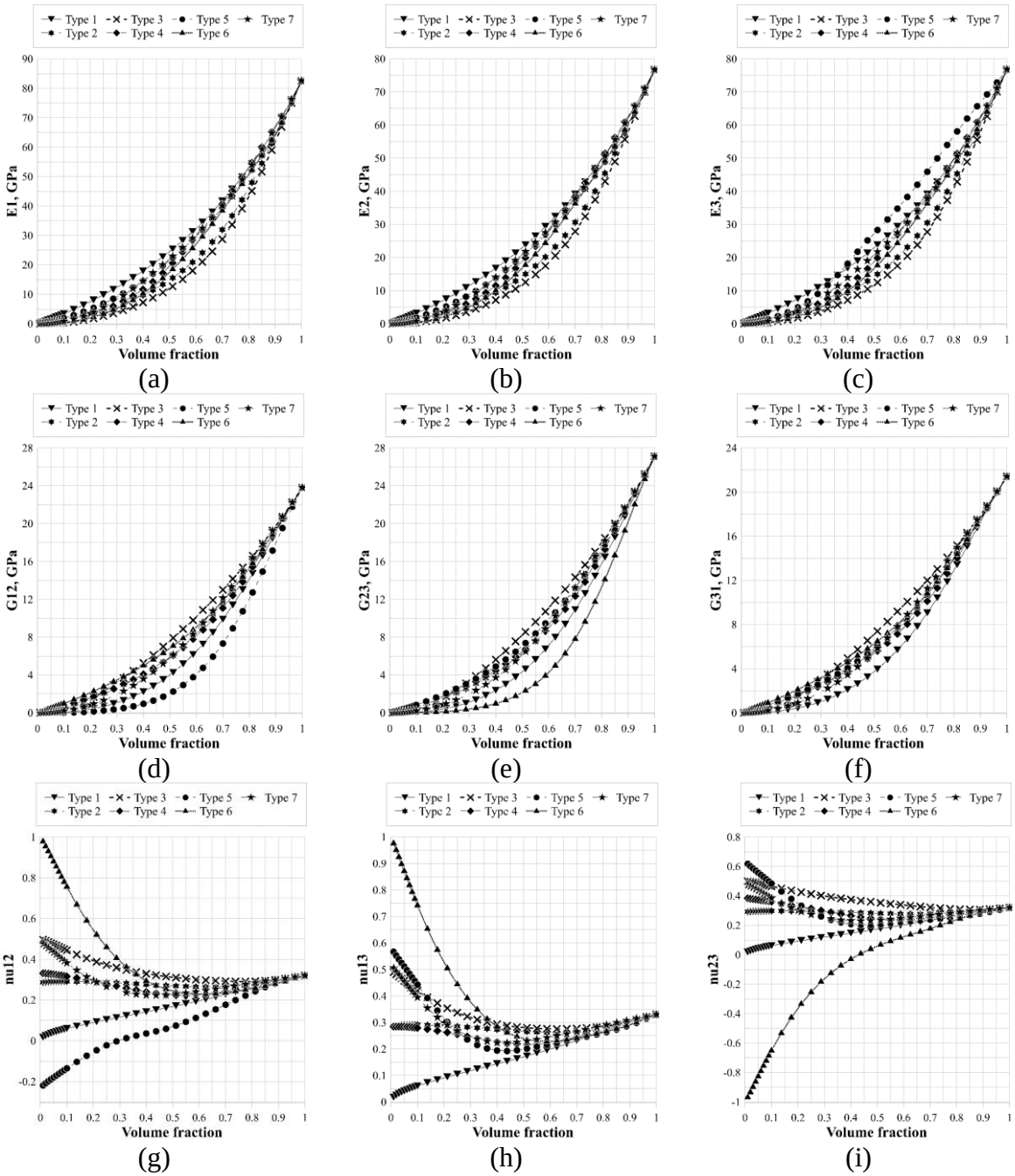

Fig. 20. Dependences of elastic constants of metamaterials formed by cells of type 1–7 on the volume fraction of solid material: (a) Young's modulus E_1, (b) Young's modulus E_2, (c) Young's modulus E_3, (d) shear modulus G_{12}, (e) shear modulus G_{23}, (f) shear modulus G_{31}, (g) Poisson's ratio ν_{12}, (h) Poisson's ratio ν_{13}, (i) Poisson's ratio ν_{23}

The dependences for most cell types have a typical nonlinear character, generally corresponding to the behaviour of porous structures with varied porosity 0. This behaviour, however, is apparently inverted, since by definition porosity and volume fraction of the material sum to 1. As follows from the theory of composites, the Young's and shear elastic moduli of the metamaterial vary from zero to the corresponding values of the solid material following some nonlinear relationship. The degree of non-isotropy associated with additive manufacturing increases slightly with increasing relative density.

The values of the mechanical characteristics of metamaterials strongly depend on the type of unit cell. We can observe from the computations that the nature of the dependence coincides with the intuitive understanding of the metamaterial behaviour, correlated with the basic concepts of deformable solid mechanics. The mechanical characteristics grow with an increase in the volume fraction, tending to the values of the moduli in the solid $AlSi_{10}Mg$ alloy. However, as seen from Figure 20, the mechanical characteristics vary at a different rate in each of the unit cells given the same variation rate of effective density.

Analysing the curves, we see a distinct dependence of the mechanical characteristics of the metamaterial on the volume fraction of the base material. When comparing the elastic moduli in each direction for all the considered cell types, the cells with the highest and the lowest elastic modulus along each of the axes are distinguished. In particular, the largest Young's modulus along the axes *X* and *Y* is observed in the cell of type 1, along the axis *Z* – by the cell of type 1 (at lower values of volume fraction) and by the cell of type 5 (at medium values of volume fraction) and by the cells of types 5 and 6 (at volume fraction close to 1). The lowest elastic modulus along each of the axes is observed in the cell of type 3.

The dependence of the parameters on the relative density of the material is similar for all of the cell types, but due to the lack of complete symmetry of some types of basic cells, some differences occur, mainly when considering the Young's modulus along *Z* axis. It is also important to mention that metamaterials based on the cells of types 3 and 4 demonstrate the effect of "sagging" of Young's modulus values at the volume fractions of 0.3–0.8. This effect might be useful in terms of selecting the optimal combination of mass and stiffness properties.

It is also interesting to note that auxetic behaviour occurs for the metamaterials of types 5 and 6, and this effect takes place over the whole considered range of the volume fraction.

Effect of unit cell asymmetry on metamaterial properties. The effect of gradual contraction of the cell along one coordinate axis (*X*) is demonstrated in Fig. 21 in the form of dependences of Young's and shear moduli and Poisson's ratio on the side length of the periodicity cell along the *X* axis. The effect of the difference of the sides of the unit cell is shown above in Figs. 10–16.

The results of finite element homogenization of the cells with different aspect ratios suggest that Young′s modulus evidently decreases along the *X* axis with the decrease in the value of the unit cell side L_x. The reason for this is the decrease in the effective cross-sectional area perpendicular to the *X* axis due to the decrease in the thickness of the rod. The values of elastic moduli along the other two axes increase. This fact can be explained, on the contrary, by the increase in the effective cross-sectional area perpendicular to the *Y* and *Z* axes. The rate of decrease of E_x is higher than the rate of increase of E_y and E_z. In the cells of types 1 and 2 the character of Young's modulus variation along each of the axes is close to linear.

It is important to mention that the basic mechanical characteristics of the metamaterial are close to isotropic before the decrease in L_x. The cell of type 6 shows a significant increase in Young's moduli along the *Y* and *Z* axes, with a slight decrease in Young's moduli along the *X* axis. In contrast, the cells of types 3 and 7 exhibit a relatively low growth of Young's moduli E_2 and E_3 and a significant decrease of E_1 with a less than twofold decrease in the parameter L_x. However, a decrease in Young's moduli along each of the three axes occurs with a further decrease in the parameter L_x.

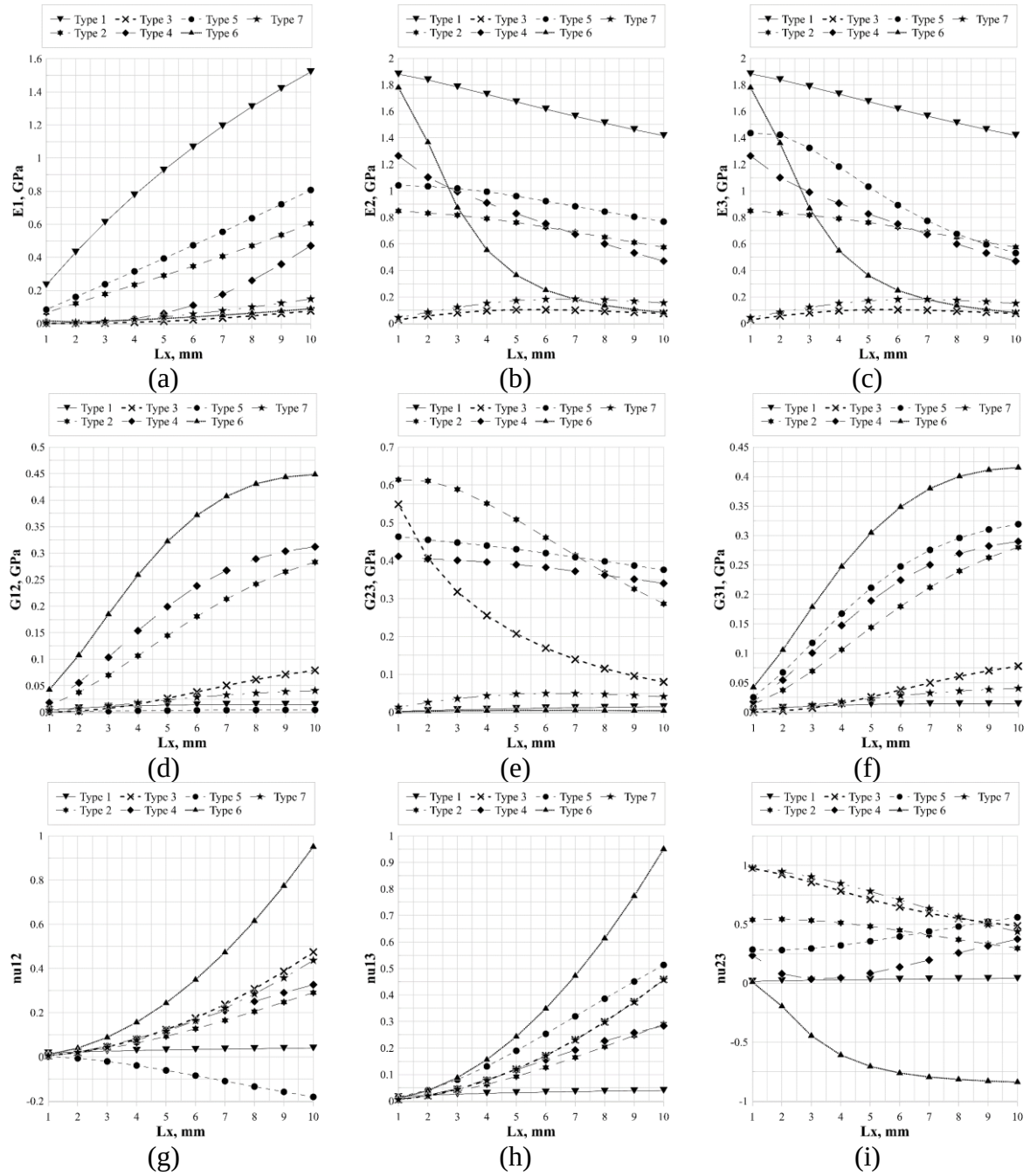

Fig. 21. Dependences of elastic properties on the length of cell side L_x for metamaterial formed by unit cells of types 1–7: (a) Young's modulus E_1, (b) Young's modulus E_2, (c) Young's modulus E_3, (d) shear modulus G_{12}, (e) shear modulus G_{23}, (f) shear modulus G_{31}, (f) Poisson's ratio ν_{12}, (g) Poisson's ratio ν_{13}, (i) Poisson's ratio ν_{23}

Since the mechanical characteristics of cells with different values of the parameter L_x were computed at a fixed material volume fraction and a constant unit cell mass, an increase in Young's moduli along the Y and Z axes can be achieved without increasing the amount of material. Thus, the stiffness of the metamaterial can be tailored to the desired level by varying the aspect ratios of the unit cell.

Elastic moduli of the metamaterial in the rotated coordinate system. Due to their geometrical features, metamaterials might have a high degree of anisotropy and have different values of mechanical characteristics in different directions. The paper considers unit cells of

each type at 0.4 vol. % (Fig. 18), and an algorithm for determining the elastic moduli in different directions is developed using Eqs. (12), (22). Surface diagrams are given as a typical example for the values of Young's modulus in different directions of the local coordinate system (Fig. 22). Such diagrams can be interpreted as the average stiffness at an arbitrary stretching direction of the metamaterial.

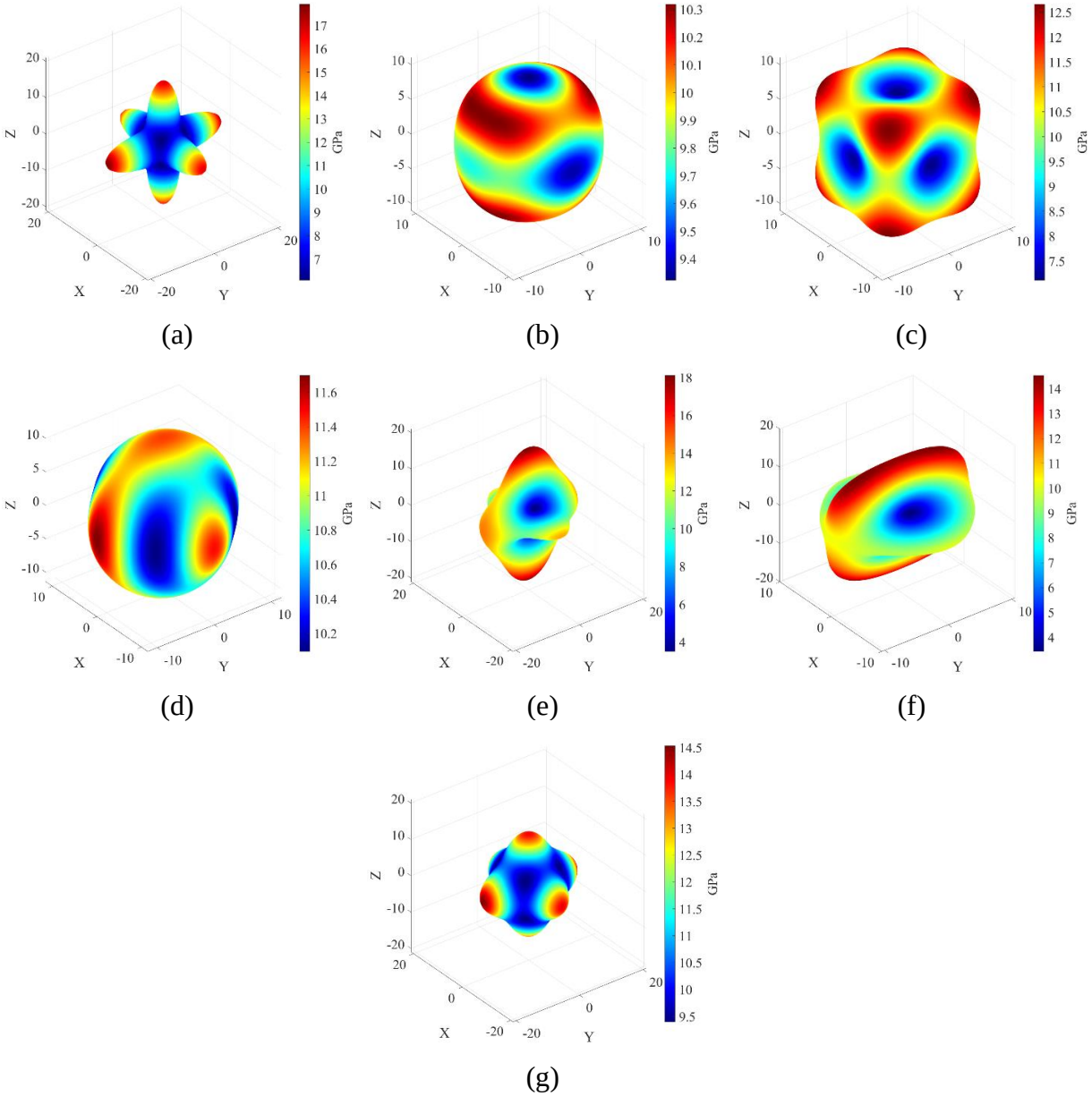

Fig. 22. Young's modulus of the metamaterial formed by cells of different types with 0.4 vol. %: (a) type 1, (b) type 2, (c) type 3, (d) type 4, (e) type 5, (f) type 6, (g) type 7

As follows from the diagrams (Fig. 22), the character of the modulus distribution depends significantly on the type of unit cell. In particular, cells of types 1 and 7 have significantly higher Young's moduli in the directions of the principal axes. Conversely, however, the cell of type 3 has a higher Young's modulus value in the diagonal direction. The diagrams for cells of types 5 and 6 show a lower amount of symmetry planes, reflecting the geometric properties of these cells, while the modulus values cover a much wider range compared to other unit cell types. Cell of types 2 and 4 have less pronounced anisotropy compared to other types of unit cells. Cells of types 5 and 6, demonstrating auxetic properties, also have a characteristic, different from classical metamaterials, appearance of circular diagrams of the Young's modulus.

Depending on the cell type, Young's modulus both increases and decreases in the direction of each of the orthogonal axes, which is well-observed in the diagrams above. Thus, cells of types 1, 5 and 7 exhibit a decrease in Young's moduli by 2–11 times in each direction when the axes are rotated. Cells of types 2, 3, 4 and 9 exhibit an increase in Young's moduli by 1.5–2.5 times for each of the axes.

Analysing the diagrams presented above for the cells whose rods are aligned with the global axes, it is possible notice an interesting feature. If we consider such rotation, which makes the axes aligned with the diagonals of the unit cell, the values taken by the diagonal components of the elastic moduli tensor decrease significantly, as well as the spread in the values of all tensor components. Conversely, a significant increase of some components corresponding to the loading direction in the new axes is observed for other cells when the direction of the changes, which suggesting that the axes are oriented more rationally under homogeneous loading.

Conclusion

Analysis of the properties of lattice structures is a burgeoning area of research in mechanics. This article describes an approach to studying the macroscopic mechanical properties of metamaterials. We formulated and verified a number of assumptions about the relationship between mechanical properties and topological parameters, such as the type of unit cell, volume fraction of material, geometrical parameters of the RVE.

We aimed to determine the overall influence of the topology of a heterogeneous periodic structure on the values of macroscopic mechanical characteristics in a metamaterial. We found the topology parameters estimating the influence that each of them has on the results of the obtained elastic moduli of the porous material.

Analysing the influence of the RVE aspect ratios, we found a significant decrease in Young's moduli in the direction of the axis along which the geometric size of the cell varied; on the other hand, a significant increase in Young's moduli along the other two axes was observed as well.

The diagrams illustrate the influence of anisotropy of the additive material used to produce the metamaterial cells on the resulting mechanical properties. Varying the direction of the local axes allows to better assess the mechanical capabilities of the unit cells by monitoring their stiffness in other directions.

Studies on a range of dependences should allow to design materials with specific mechanical properties, required for developing modern advanced industrial products based on continuum mechanics, mechanics of heterogeneous media and composites, computational mechanics and mathematical modelling, biomedical and advanced manufacturing technologies.

References

1. Lewandowski JJ, Mohsen S. Metal additive manufacturing: A review of mechanical properties. *The Annual Review of Materials Research*. 2016;46(1): 151–186.
2. Hanks B, Berthel J, Frecker M, Simpson TW. Mechanical properties of additively manufactured metal lattice structures: Data review and design interface. *Additive Manufacturing*. 2020;35: 101301.
3. Maslov LB. Dynamic Model of a Periodic Medium with Double Porosity. *Mechanics of Solids*. 2018;53: 184–194.
4. Omairey SL, Dunning PD, Sriramula S. Development of an ABAQUS plugin tool for periodic RVE homogenisation. *Engineering with Computers*. 2019;35: 567–577.
5. Christensen J, Kadic M, Kraft O. Vibrant times for mechanical metamaterials. *MRS Communications*. 2015;5(3): 453–462.
6. Oraib A, Rowshanc R, Rashid K. Topology-mechanical property relationship of 3D printed strut, skeletal, and sheet based periodic metallic cellular materials. *Additive Manufacturing*. 2018;19: 167–183.

7. Bin RS, Mazedur RM. Modeling elastic properties of unidirectional composite materials using Ansys Material Designer. *Procedia Structural Integrity*. 2020;28: 1892–1900.
8. Zadpoor AA. Mechanical meta-materials. *Materials Horizons*. 2016;3(5): 371–381.
9. Gibson LJ, Ashby MF. *Cellular solids: structure and properties*. Cambridge University Press. 1997.
10. Hedayati R, Sadighi M, Mohammadi-Aghdam M, Zadpoor A. Mechanical behavior of additively manufactured porous biomaterials made from truncated cuboctahedron unit cells. *International Journal of Mechanical Sciences*. 2016;106: 19–38.
11. Deshpande V, Ashby M, Fleck N. Foam topology: bending versus stretching dominated architectures. *Acta Materialia*. 2001;49(6): 1035–1040.
12. Zadpoor AA, Hedayati R. Analytical relationships for prediction of the mechanical properties of additively manufactured porous biomaterials. *Journal of Biomedical Materials Research Part A*. 2016;104(12): 3164–3174.
13. Hedayati R, Sadighi M, Mohammadi-Aghdam M, Zadpoor A. Mechanical properties of regular porous biomaterials made from truncated cube repeating unit cells: analytical solutions and computational models. *Material Science and Engineering*. 2016;60: 163–183.
14. Wauthle R, Vrancken B, Beynaerts B, Jorissen K, Schrooten J, Kruth J-P, Van Humbeeck J. Effects of build orientation and heat treatment on the microstructure and mechanical properties of selective laser melted Ti6Al4V lattice structures. *Additive Manufacturing*. 2015;5: 77–84.
15. Wang Y, Zhang L, Daynes S, Zhang H, Feih S, Wang MY. Design of graded lattice structure with optimized mesostructures for additive manufacturing. *Materials and Design*. 2018;142: 114–123.
16. Loh GH, Pei E, Harrison D, Monzón MD. An overview of functionally graded additive manufacturing. *Additive Manufacturing*. 2018;23: 34-44.
17. Lee J-H, Singer JP, Thomas EL. Micro/Nanostructured Mechanical Metamaterials. *Advanced Materials*. 2012;24(36): 4782–4810.
18. Kolken HMA, Zadpoor AA. Auxetic mechanical metamaterials. *RSC Advances*. 2017;7(9): 5111–5129.
19. Wallbanks M, Khan MF, Bodaghi M, Triantaphyllou A, Serjouei A. On the design workflow of auxetic metamaterials for structural applications. *Smart Materials and Structures*. 2021;31(2): 023002.
20. Zhmaylo M, Maslov L, Borovkov A, Tarasenko F. Finite element homogenization and experimental evaluation of additively manufactured lattice metamaterials. *Journal of the Brazilian Society of Mechanical Sciences and Engineering*. 2023;45: 299.
21. *SolidWorks Help*. Available from: https://help.solidworks.com/2023/English/SolidWorks/sldworks/r_welcome_sw_online_help.htm [Accessed 11th August 2022].
22. Maslov LB. *Finite element poroelastic models in biomechanics*. St. Petersburg: Lan' Publ. House; 2023. (In-Russian)
23. Maslov LB. Biomechanical model and numerical analysis of tissue regeneration within a porous scaffold. *Mechanics of Solids*. 2020;55(7): 1115–1134.

THE AUTHORS

A.I. Borovkov
e-mail: borovkov@compmechlab.com

L.B. Maslov
e-mail: leonid-maslov@mail.ru

M.A. Zhmaylo
e-mail: zhmaylo@compmechlab.com

F.D. Tarasenko
e-mail: tarasenko@compmechlab.ru

L.S. Nezhinskaya
e-mail: nezhinskaya.l@compmechlab.ru